

# 16-Ports Indoor Base Station MIMO Array for Sub-6 GHz 5G Applications

**Tamer Gaber Abouelnaga**

KFS Higher Institute of Engineering

**Ibrahim Zewail** (✉ [Eng\\_ibrahimzewail@yahoo.com](mailto:Eng_ibrahimzewail@yahoo.com))

kfs Higher Institute for Engineering and Technology <https://orcid.org/0000-0002-8127-0920>

**Mona Shokair**

Menoufia University

---

## Research Article

**Keywords:** 5G, MIMO, Indoor base station (BS), ergodic capacity

**Posted Date:** January 27th, 2022

**DOI:** <https://doi.org/10.21203/rs.3.rs-1206420/v1>

**License:** © ⓘ This work is licensed under a Creative Commons Attribution 4.0 International License.

[Read Full License](#)

---

# 16-ports Indoor Base Station MIMO Array for Sub-6 GHz 5G Applications

Tamer Gaber Abouelnaga<sup>1</sup>, Ibrahim Zewail<sup>2</sup> and Mona Shokair<sup>3</sup>

<sup>1</sup> Microstrip Circuits Department, Electronics Research Institute (ERI), Cairo, Egypt

<sup>1,2</sup> Higher Institute of Engineering and Technology, Kafr El-Shiekh, Egypt

<sup>3</sup> Faculty of Electronic Engineering, El-Menoufia University, Menouf, 32952, Egypt

E-mail address: tamer@eri.sci.eg, eng\_ibrahimzewail@yahoo.com, and mona.sabry@el-eng.menofia.edu.eg

## Abstract

A typical 5G multiple-input and multiple-output (MIMO) system must combine a high number of antennas at both the transmitter and receiver to realize spatial multiplexing capability. In this paper, a wideband 16-element indoor base station (BS) antenna array that can cover 3.3–6.0 GHz is proposed for 5G applications. A  $\pi$ -shaped monopole antenna is designed to cover the Lower band (LTE bands 42/43 - N77 - N78), the intermediate band (N79), and the higher band (LTE 46). The antenna elements are arranged in a limited space printed on a substrate takes the Hexakaidecagon Polygon shape. Where, the antenna elements are arranged with good isolation, achieving good polarization diversity. The proposed BS array is simulated, fabricated, and tested. The typical results, S-parameters, antenna efficiency, and radiation patterns are investigated. Moreover, to validate the MIMO performances, a very low envelope correlation coefficient (ECC) below 0.02, high antenna efficiency of about 82% - 93.2% are achieved. The calculated ergodic channel capacity of the 16×16 MIMO system reached up to 85 bps/Hz. A comparison between the proposed antenna array and some other 5G MIMO indoor base station antennas is studied.

**Key Words:** 5G, MIMO, Indoor base station (BS), ergodic capacity

## I. Introduction

The 5th generation of communication technology has several advantages over the present 4G system, including a greater transmission rate and lower latency [1]. Furthermore, it has been proved that a multiple-input multiple-output (MIMO) system with a reasonably large number of antennas elements should be used to achieve high throughput for 5G operations below 6 GHz [2]. To accomplish high-order diversity and multiplexing, a large number of antenna components should be incorporated in the user equipment (UE) [3] and the base station (BS)[4],[5].

In general, increasing the number of antennas poses a challenge for both the indoor Base Station (BS) and the user equipment. On the one hand, antenna volumes are highly constrained, making degradations in isolation and antenna efficiency difficult to prevent [6],[7]. On the other hand, new potential sub-6 GHz bands must be covered in addition to the well-known 3.5-GHz C band (3400-3600 MHz, LTE band 42). For 5G, it is now necessary to research multimode and multi-band MIMO systems. 3GPP has revealed that the 5G New Radio (NR) [8] will have three sub-6GHz operating bands: N77 (3.3-4.2GHz), N78 (3.3-3.8GHz), and N79 (3.3-3.9GHz) (4.4-5.0GHz). From the three bands listed above, countries can choose their own 5G bands.

Many 5G MIMO array designs have recently been proposed. For MIMO indoor base station applications, a four-port wide-band antenna with unidirectional and independent radiation patterns is described [9]. Where this design is made up of four T-shaped monopoles that are grouped in an orthogonal and symmetrical pattern. To improve the isolation between ports, an X-shaped isolating block is inserted in the cavity's center. In ref [10], for 5G base station applications, a coaxial CTS array antenna based on SICL technology is proposed. The proposed antenna can be made by stacking many substrates together using SICL as the transmission line. As a result, the SICL-CTS array antenna has a very high level of integration. In [11], proposed a base station antenna design. We use microstrip antennas, which are increasingly commonly used due to their low weight and small footprint, and have a narrow bandwidth and modest gain, in this work's suggested antenna array, which operates at 28 GHz and spans the millimeter-wave range.

A design method for aperture-type antennas is described in [12], as well as multi-beam emission patterns. An offset dual reflector is used for the reflector antenna. The method for increasing the radiation pattern using reflector shaping is described. Shaped lens antennas are used in dielectric lens antennas. The method for increasing the radiation pattern by lens shaping is described. In [4], a design for the BS and UE, offer two multimode and multiband 5G MIMO antenna array, respectively. The BS antenna array consists of eight isolated MIMO antennas that cover a frequency range of 3.4-7.1 GHz. also, two types of protruded parasitic devices are developed to aid in mutual coupling reduction. In ref. [13] a dual-polarized wideband Vivaldi antenna was proposed for 5G base stations. Two perpendicularly polarized Vivaldi elements are used to create dual-polarization. The design was proposed to cover a 1.4-3.8GHz band which is limited compared to other designs.

In ref. [14], a tightly coupled structure is used to propose a dual-polarized cross-dipoles base station antenna. The antenna's impedance bandwidth is substantially broadened by the coupling effect between the orthogonal dipoles. A concept for down-tilted 3D Taper Slot Antennas that could be used in future mobile communication base stations was introduced in [15]. A cavity-backed broadband high-efficiency antenna with distinct beams is presented [16], because of its four independent beams, this antenna is a compact and low-cost option that can be simply built to be deployed as a 5G indoor base station antenna. In ref. [17], for 2G/3G/LTE systems, a dual-broadband MIMO indoor base station antenna was proposed to cover the frequency bands (800 - 960 MHz) and (1700 - 2700 MHz). The design has a low profile and simple feeding structure, but only two antenna elements were proposed to achieve MIMO operation and it can't cover higher frequency bands.

In this paper, a wideband 16- element indoor base station antenna array is proposed for 5G applications. A  $\pi$ -shaped monopole antenna is designed to cover the Lower band (LTE bands 42/43 - N77 - N78), the intermediate band (N79), and the higher band (LTE 46). The novelty of the paper lies in using 16 antenna elements in a limited space printed on a substrate that takes the Hexakaidecagon Polygon shape. Where antenna elements are arranged with good isolation, polarization diversity and pattern diversity are attained. The typical results, S-parameters, antenna efficiency, and radiation patterns are investigated. Moreover, to validate the MIMO performances, very low envelope correlation coefficient (ECC) value, high antenna efficiency, and high channel capacity are achieved. The proposed BS array is simulated, fabricated, and tested. Lastly, a detailed comparison of the proposed antenna array and some 5G MIMO indoor base station antennas are studied.

## II. Proposed Antenna Array Design

### A. Array Structure

In this section, a 16-element BS MIMO antenna array is presented. As shown in Figure 1, the system circuit board (substrate) is a Hexakaidecagon Polygon shape fabricated from FR4 material (with relative permittivity 4.4 and loss tangent 0.02). The FR4 substrate has a dimension of 140mm  $\times$  140mm  $\times$  1.5mm. The hexakaidecagon substrate has 16 sides and an Interior Angle of 157.5°. The BS antenna elements are identical and arranged, on the front surface of the substrate.

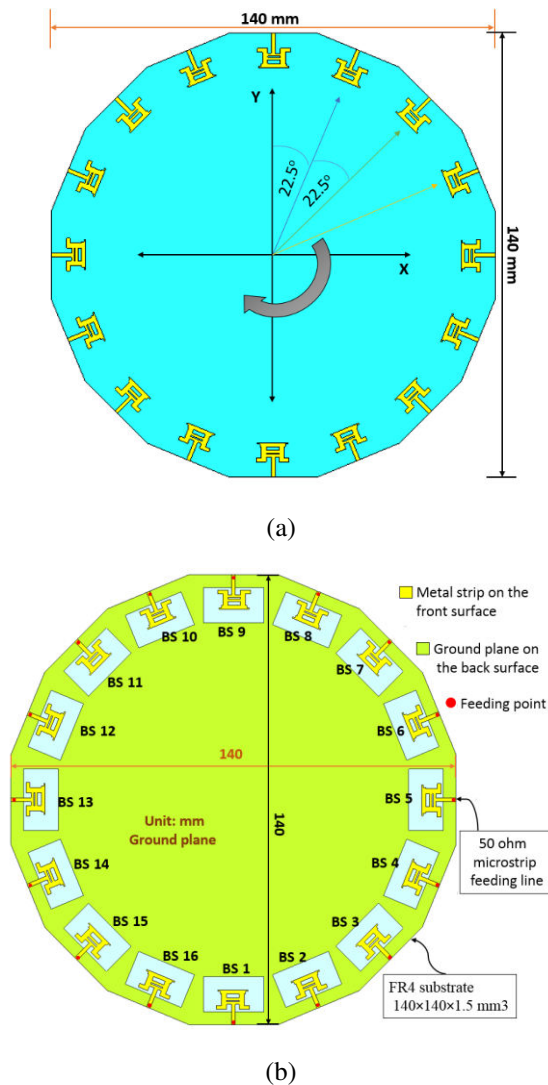


Figure 1 Geometry and dimensions of the proposed indoor 16- BS MIMO array. (a) Top view and (b) detailed structure of the ground plane and the decoupling structures

As depicted in Figure 1 (A), each BS antenna is printed at each side of the hexakaidecagon, where the angle between every two adjacent antenna elements center is 22.5°. A ground plane is also printed on the back surface of this substrate. As shown in Figure 1 (B), the ground plane is formed by rectangle slots with dimensions 19 mm  $\times$  11 mm. Moreover, forming the ground plane helps to mitigate the mutual coupling between antenna elements.

### B. Antenna Element

The structure and dimension of the BS antenna element are shown in Figure 2 (a). A conventional multi-branch monopole is used as the BS antenna element, fed with a 50  $\Omega$  micro strip line. The antenna track is formed to produce a new  $\pi$ -shaped. The various radiators' resonant modes can be coupled to cover a frequency range of 3.3-6 GHz. The proposed antenna's bandwidth is sufficient to facilitate MIMO operation in most sub-6 GHz 5G channels, including the LTE bands 42/43 (3.4-3.8 GHz), LTE 46 (5.15-5.925 GHz), also the new radio bands N77 (3.3-4.2GHz), N78 (3.3-3.8 GHz), and N79 (4.4-5.0GHz). The proposed antenna introduces a compact size as compared to the conventional printed monopole antenna.

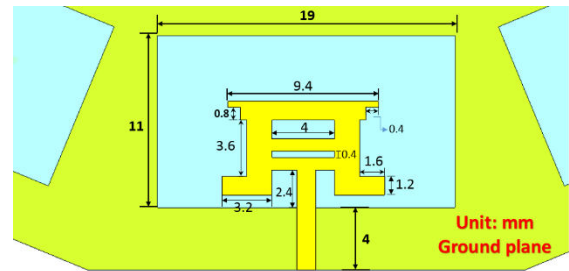


Figure 2 detailed structure of the BS antenna element

Figure 3 illustrates the simulated surface current distribution of a single antenna element at 5.25 GHz. The current distributions is shown to have a peak value at the antenna's Line and a null at the antenna element's margins. Also, the current distributions is shown to be dispersed around the slot. The resonance frequency is considered as the

fundamental mode generated by the antenna shape and the slot.

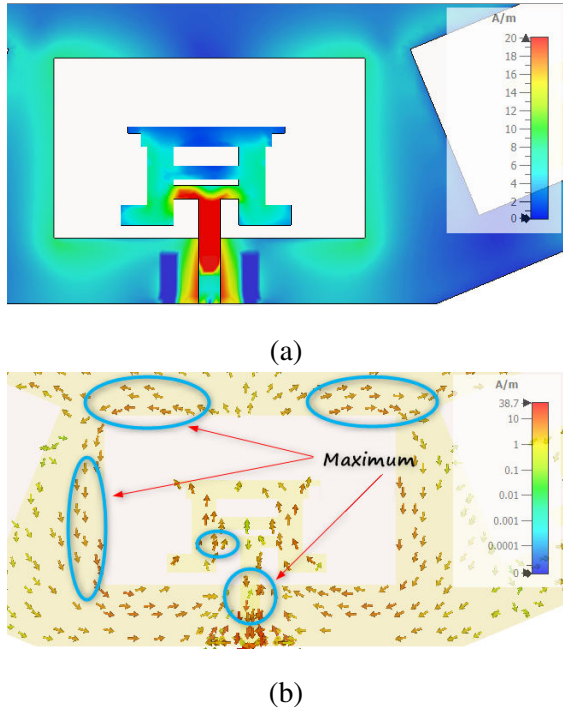


Figure 3 (a), (b) Simulated surface current distributions of Ant 1 at 5.25 GHz

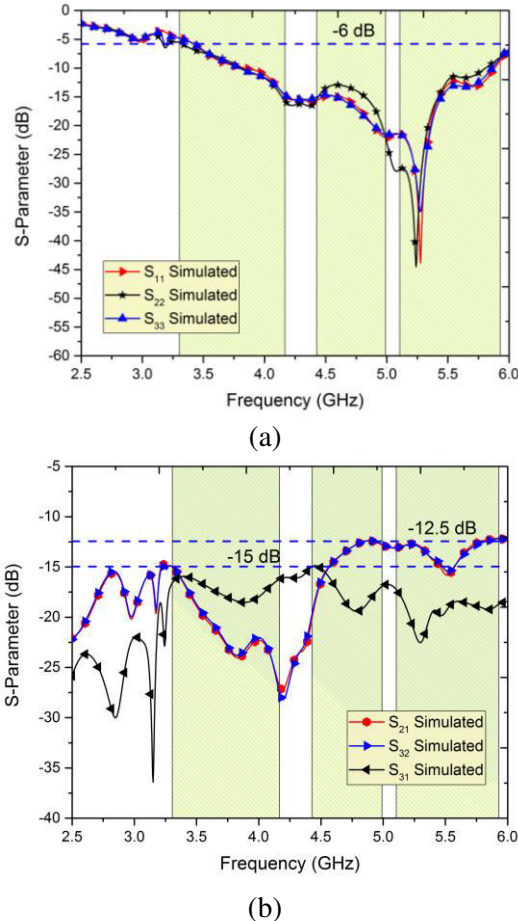


Figure 4 Simulated S-parameters. (a) Reflection coefficients and (b) transmission coefficients

The suggested BS MIMO antenna array's simulated S-parameters (reflection coefficients and transmission coefficients) are shown in Figure 4. Only the reflection coefficients of Ants 1-3 are presented due to the symmetry of the array structure. Where it represents a quarter of the proposed array. It is revealed that the suggested antenna array has good return losses of more than 6 dB over the entire bandwidth of 3.3-6 GHz. The simulated results in figure 4 (a) indicate a -6 dB fractional bandwidth of 51.43 % (3.3 – 6 GHz).

In Figure 4 (b), the isolations between any two non-adjacent antennas are acceptable (>17.5 dB), This is due to sufficient separation between the antenna elements, where the simulated S31 is even lower than -16 dB, -15 dB, and -17.5 dB, through (LTE bands 42/43 - N77 - N78), N79, and LTE 46 respectively. Also, the isolations between two neighboring antennas are provided. Where S21 and S32 are symmetric and lower than -12.57 dB, -12.5 dB, and -12.29 dB, (LTE bands 42/43 - N77 - N78), N79, and LTE 46 respectively. This behavior is reasonable because the angle between any two adjacent antenna elements is  $22.5^\circ$  that yields polarization with angle, and thus achieves the feature of dual-polarization.

### III. Antenna Prototype and Measurement results

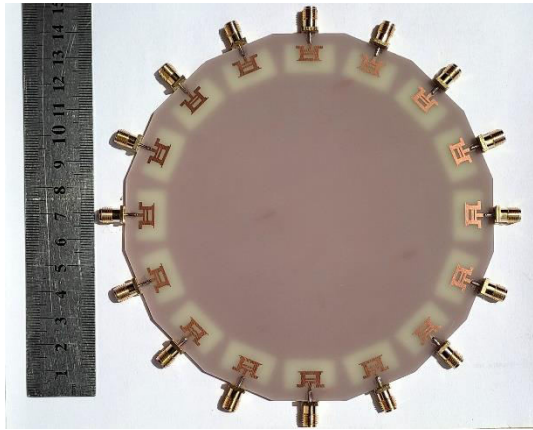
#### A. Antenna Fabrication

A prototype is fabricated to test the feasibility of the proposed indoor BS, 16-element MIMO antenna array, as illustrated in Figure 5.

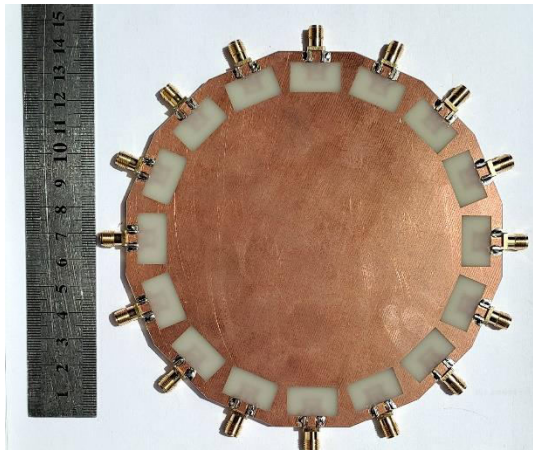
#### B. Reflection Coefficients

Due to fabrication errors as misalignment between the antenna element and its slot in the ground plane, antenna elements are very similar to each other but not a replica, figure 6 (a) shows that the proposed BS antenna array may operate in the ultra-wideband range of 3.3-6 GHz with a return loss of more than 6 dB of 49 % (3.75–6 GHz), 70 % (3.75–7 GHz)

and 57 % (3.3– 5.925 GHz) for  $S_{11}$ ,  $S_{22}$ , and  $S_{33}$  respectively. Moreover, as shown in Figure 6 (b) the proposed isolation for  $S_{21}$  and  $S_{32}$  of more than 15 dB and 12.7dB through the lower band and higher band respectively. The isolation for the non-adjacent antennas  $S_{31}$  is more than 25 dB and 18 dB through the lower band and higher band, respectively.

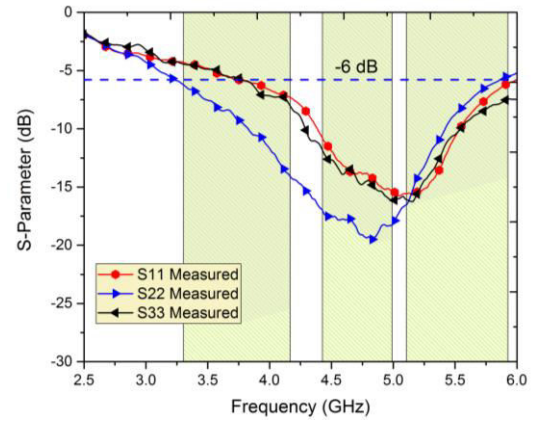


(a)

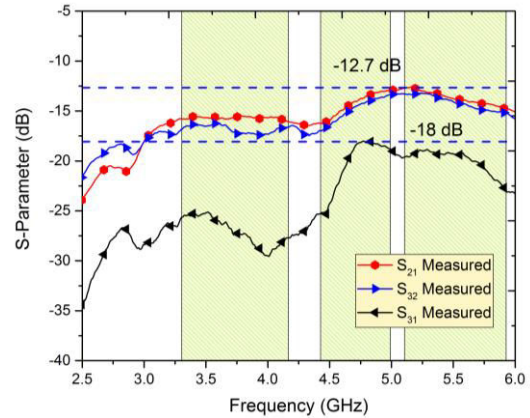


(b)

Figure 5 photograph of the fabricated prototype indoor BS 16-element MIMO array. (a) front view (b) back view



(a)



(b)

Figure 6 Measured S-parameters. (a) Reflection coefficients, (b) isolation (for Ants 1, 2 and 3),

Due to the structure symmetry, the reflection coefficients ( $S_{11}$ ,  $S_{22}$ , and  $S_{33}$ ) are measured of Ants 1–3 as shown in Figure 6 (a). There is a slight difference between the measured and simulated results may due to minor fabrication errors, misalignment, the insertion loss of the SMA connector, and tolerances.

### C. Isolations and ECCs

The envelope correlation coefficient (ECC) and channel capacity (CC) of the proposed wideband 16-element BS MIMO system will be examined to further show the performance of the proposed system.

For simplification, to compute the ECC value, the multipath environment is considered to be isotropic in terms of both polarizations and power density [1]. As a result, the complex radiation far field may compute the envelope correlation between two antennas  $i$  and  $j$  as follows:

$$ECC(i, j) = \frac{|\oint A_{ij}(\theta, \varphi) \sin \theta d\theta d\varphi|^2}{\oint |A_{ii}(\theta, \varphi) \sin \theta d\theta d\varphi| \cdot \oint |A_{jj}(\theta, \varphi) \sin \theta d\theta d\varphi|} \quad (1)$$

$$A_{ij}(\theta, \varphi) = E_{\theta, i}(\theta, \varphi) \cdot E_{\theta, j}^*(\theta, \varphi) + E_{\varphi, i}(\theta, \varphi) \cdot E_{\varphi, j}^*(\theta, \varphi) \quad (2)$$

Fig. 7 illustrates the simulated ECC of the proposed MIMO system. Where the value of ECC is computed from the complex radiation far-field of the antennas acquired directly from CST for every two adjacent antenna elements.

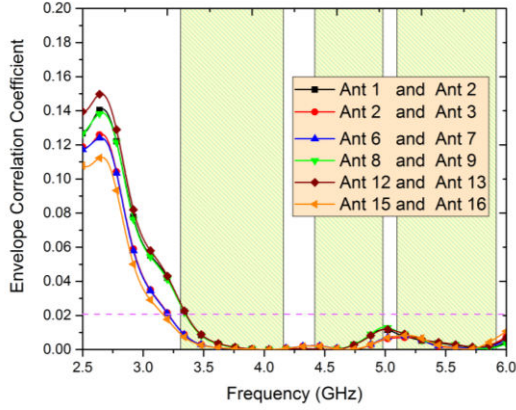


Figure 7 Simulated envelope correlation coefficient (ECC)

As demonstrated in Figure 7, the simulated ECC value is less than 0.02 over the whole band 3.3-6 GHz, and very close to 0 across 3.5-4.75 GHz and across 5.5 - 5.925 GHz which is sufficient for 5G MIMO operation.

#### D. Total Antenna Efficiency

Fig. 8 shows the simulated total efficiency of the proposed 16 port BS MIMO structure. Due to the symmetry structure, only the simulated efficiencies of Ant1 – Ant8 are shown for brevity. As shown in Figure 8, one can note that the efficiencies for all antenna elements are near each other. Where the efficiency in the lower band (LTE bands 42/43 - N77 - N78) ranges from 89% to 93.2% and in the intermediate band (N79) ranges from 88.2% to 92.1%, and in the higher band (LTE 46) ranges from 82% to 89.3%.

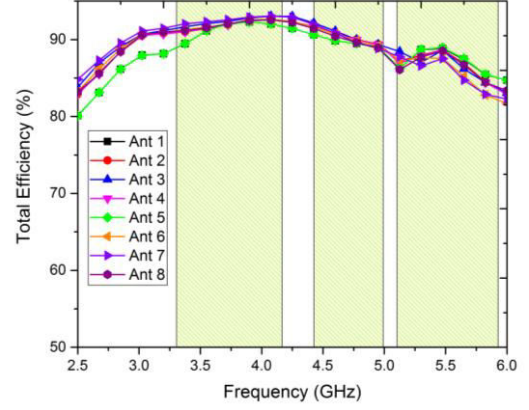
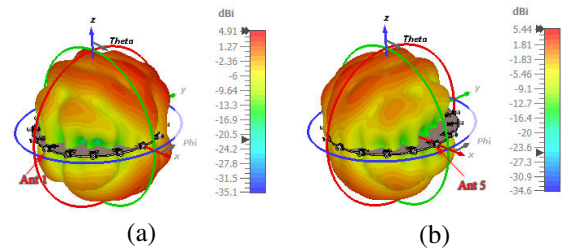


Figure 8 Simulated total efficiency of the proposed system

#### E. RADIATION PERFORMANCES

In this section, we investigate the radiation patterns of Ants 1, 5, 9, and 13. For brevity, the radiation patterns of other antenna elements are not presented here due to the symmetrical arrangement of MIMO antenna systems. Where Figure 9 depicts the simulated 3-dimensional radiation pattern of Ants 1, 5, 9, and 13 at 5.2 GHz. The radiation patterns of the antennas are symmetrical and rotate by angle 45o according to the antenna number. As in Figure 9, the maximum radiation direction of Ant1 is tilted and pointed to + y-axis at 5.2 GHz. Also, the maximum radiation direction of Ant 5 is pointed to - X-axis. For Ants 9 and 13, the radiation patterns are at opposite directions of ants 1 and 5 respectively. thereby demonstrating the pattern diversity feature.



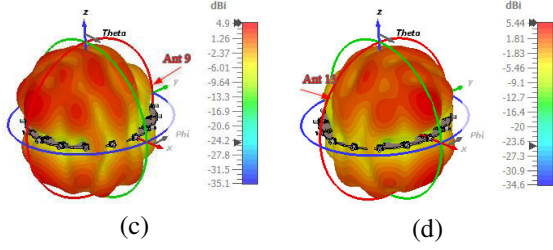


Figure 9 Simulated 3D radiation patterns, (a) Ant 1, (b) Ant 5, (c) Ant 9, (d) Ant 13, at 5.2 GHz

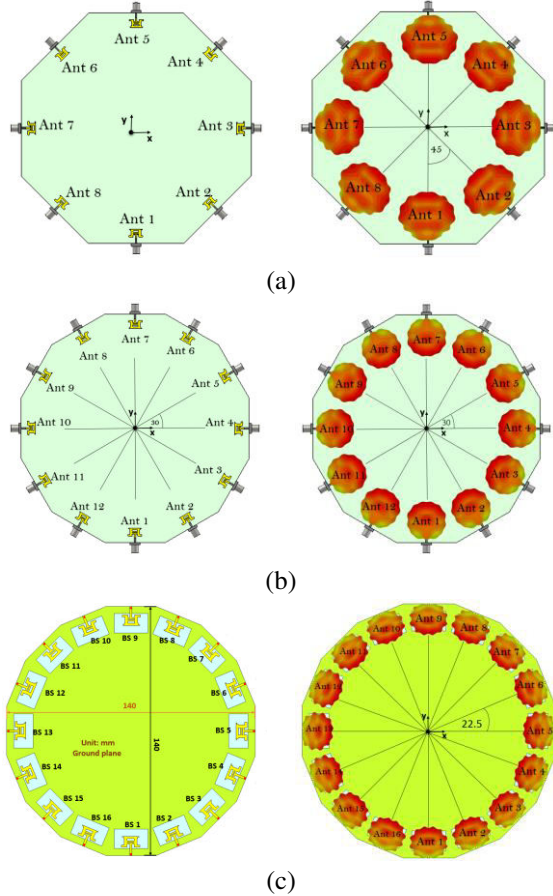


Figure 10 Three different substrate shapes: (a) Octagon Polygon shape, (b) Dodecagon Polygon shape, and (c) Hexakaidecagon Polygon shape.

Figure 10 shows the effect of changing the orientation of array elements which results in the rotation of the radiation patterns. Figure 10 (a) presents the Octagon Polygon shape which has 8 sides with 8 antenna elements. The angle between every two adjacent antennas (rotation angle) is  $45^\circ$ . So that the radiation pattern is rotated by the same angle. Also, in figure 11 (b) the Dodecagon Polygon shape is shown, which has 12 sides with 12 antenna elements, with a rotation angle equal to  $30^\circ$ . In this

paper, we used the Hexakaidecagon Polygon shape that has 16 sides with 16 antenna elements, with a rotation angle of  $22.5^\circ$ . Thereby achieving good pattern diversity and better MIMO performances.

#### F. Channel Capacity (CC)

The channel capacity (CC) is evaluated as:

$$CC = E \left\{ \log_2 \left[ \det \left( I + \frac{SNR}{n_T} H H^T \right) \right] \right\} \quad (3)$$

Where  $E$  indicates the expectation for various channel realizations,  $I$  is an identity matrix, SNR is the mean signal-to-noise ratio at the receiving end,  $n_T$  is the number of transmitting antennas,  $(.)^T$  is the Hermitian transpose and the  $H$  channel matrix can be computed as follows:

$$H = \sqrt{\rho_{RX}} H_{i.i.d} \sqrt{\rho_{TX}} \quad (4)$$

Where  $\rho_{RX}$  and  $\rho_{TX}$  are the correlation coefficient matrices of the receive and transmit antenna, respectively, and  $H_{i.i.d}$  is the instantaneous white channel matrix. Moreover, as mentioned in [18], when calculating the channel capacity of a MIMO antenna system, the antenna overall efficiency must be taken into account:

$$\rho_{RX} = \sqrt{\eta_{total}} \cdot \rho \cdot \sqrt{\eta_{total}} \quad (5)$$

Which has the positive square root of  $\eta_{total}$  weighted by  $\rho$ . The channel capacity demonstrated in Fig. 11 is realized by assuming that the transmitting antennas are considered to be uncorrelated ( $ECC = 0$ ) and receive equal power. Moreover, the propagation scenario is independent, and equally distributed (i.i.d.) Rayleigh-fading channel with an SNR of 20 dB at the receiver end.

The proposed 16 x16 array's ergodic channel capacity is averaged across 100,000 channel realizations. The ideal channel capacity of 2 x 2 and 16 x16 MIMO systems

are computed with all antenna components at the transmitter and receiver being uncorrelated and lossless, with antenna efficiency equal to 100 % and zero-correlation coefficient.

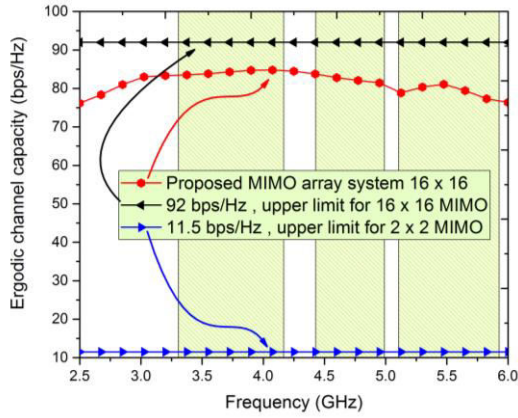


Figure 11 Calculated ergodic channel capacities of the proposed  $16 \times 16$  MIMO system (SNR = 20 dB).

The simulated channel capacities of the proposed  $16 \times 16$  MIMO system are 83.34–85 bps/Hz in the low band (LTE bands 42/43 - N77 - N78) and 81.5 – 83.8 bps/Hz in the intermediate band (N79) and 77 – 81.5 bps/Hz in the high band (LTE 46). Peak ergodic channel capacity reached 85 bps/Hz which is 7.39 times the maximum limit (11.5 bps/Hz) for a  $2 \times 2$  MIMO system.

#### IV. Performance comparison

Table 1 shows a detailed comparison of the proposed antenna array and some 5G MIMO

indoor base station antennas. The proposed array design consists of 16 antenna elements, which is twice the number of elements in [3] of the same size, with an acceptable isolation value. By comparing the antenna efficiency, the proposed antenna element has an efficiency of 93.2 %, which is better than other antennas in [3], [8], and [15]. In terms of Isolation, the isolation between any two adjacent antennas is 12.7 dB which is lower than [3] and [8]. This is because the number of antenna elements used in the proposed design is much greater than the designs in [3], and [8]. By comparing the antenna element sizes, the antenna element of the proposed MIMO array has a low planar size of 10.4 mm  $\times$  10.8 mm, which is much smaller compared to the others antennas in [3], [8], and [15].

Considering the MIMO order, the proposed array can support  $16 \times 16$  MIMO applications, and its peak channel capacity is 85 bps/Hz which is higher than the achievable capacities of the  $8 \times 10$  MIMO antenna arrays (43.3 bps/Hz) that have been reported in [3]. Furthermore, the obtained capacity is even better than the  $4 \times 4$  antenna array in [8]. Lastly, the proposed antenna array possesses an ECC value of 0.02 which is very good compared to the antennas reported in [8], [15]. But, is higher than the reported in [3], due to the number of array elements.

Table 1 performance comparison between the proposed array and other previous work

Reference	Ground size (mm <sup>3</sup> )	Bandwidth (GHz)	Efficiency (%)	Isolation (dB)	Antenna element size (mm x mm)	No of Elements	ECC	Peak channel capacity (bps/Hz)
<b>Proposed</b>	<b>140 x 140 x 1.5</b>	<b>3.3 - 6</b>	<b>82 - 93.2</b>	<b>-15</b>	<b>10.4 x 10.8</b>	<b>16</b>	<b>0.02</b>	<b>85 (16 x 16)</b>
[4]	140 x 140 x 0.8	3.4-7.1	55 - 83	-15 dB	14 x 16.5	8	0	43.3 (8 x 10)
[9]	129.5 $\times$ 129.5 $\times$ 28.2	1.55-6	84%	-16	23.15 x 20.8	4	0.5	25 (4 x 4)
[16]	75 x 75 x 18.75	3 - 5	67%	-11 dB	4.31 x 14.22	4	-	-

#### V. Conclusion

In This paper, a novel wideband 16-element indoor BS antenna array that can cover 3.3–6.0 GHz was proposed for 5G applications. A  $\pi$ -shaped monopole antenna was designed to cover the Lower band (LTE bands 42/43 - N77 - N78), the intermediate band (N79), and the higher band (LTE 46). The antenna elements were arranged in a limited space printed on a substrate takes the Hexakaidecagon Polygon shape achieving polarization diversity. Both simulation and measurement validated the performance of the 16-antenna BS MIMO system, and good MIMO antenna performance was attained. The proposed BS MIMO system show quite high isolation, antenna efficiency about 82% - 93.2%, and ECC below 0.02, which were good enough for a practical 5G MIMO indoor base station. The calculated ergodic channel capacity of the 16×16 MIMO system reached up to 85 bps/Hz. Because of the foregoing, the suggested 16-antenna BS MIMO system might be a good choice for 5G MIMO applications in indoor base stations.

## VI. References

- [1] J. C. Z. Jeffrey G. Andrew, Stefano Buzzi, Wan Choi, Stephen V. Hanly, Angel Lozano, Anthony C. K. Soong, "What Will 5G Be?," *Ieee J. Sel. Areas Commun.*, vol. 32, no. 6, pp. 1065–1083, 2014.
- [2] I. Al-Mejibli and S. Al-Majeed, "Challenges of using MIMO channel technology in 5G wireless communication systems," *2018 Majan Int. Conf.*, pp. 1–5, 2018, doi: 10.1109/mintc.2018.8472778.
- [3] T. G. Abouelnaga, I. Zewail, and M. Shokair, "Design of 10 ×10 Massive MIMO Array in Sub-6GHz Smart Phone for 5G Applications," *Prog. Electromagn. Res. B*, vol. 91, no. February, pp. 97–114, 2021, doi: 10.2528/PIERB21010304.
- [4] Y. Li and G. Yang, "Dual-mode and triple-band 10-antenna handset array and its multiple-input multiple-output performance evaluation in 5G," *Int. J. RF Microw. Comput. Eng.*, vol. 29, no. 2, pp. 1–15, 2019, doi: 10.1002/mmce.21538.
- [5] H. Xu, H. Zhou, S. Gao, H. Wang, and Y. Cheng, "Multimode Decoupling Technique with Independent Tuning Characteristic for Mobile Terminals," *IEEE Trans. Antennas Propag.*, vol. 65, no. 12, pp. 6739–6751, 2017, doi: 10.1109/TAP.2017.2754445.
- [6] H. H. Yang and T. Q. S. Quek, "Massive MIMO for Interference Suppression: Cell-Edge Aware Zero Forcing," pp. 9–34, 2017, doi: 10.1007/978-3-319-43715-6\_2.
- [7] S. X. Ta, D. M. Nguyen, K. K. Nguyen, C. Dao-Ngoc, and N. Nguyen-Trong, "A Tripolarized Antenna with Ultrawide Operational Bandwidth," *IEEE Trans. Antennas Propag.*, vol. 68, no. 6, pp. 4386–4396, 2020, doi: 10.1109/TAP.2020.2972626.
- [8] "5G NR (New Radio). Accessed: Dec. 12, 2018. [Online]. Available: <http://3gpp.org/>."
- [9] J. Molins-Benlliure, E. Antonino-Daviu, M. Cabedo-Fabres, and M. Ferrando-Bataller, "Four-Port Wide-Band Cavity-Backed Antenna with Isolating X-Shaped Block for Sub-6 GHz 5G Indoor Base Stations," *IEEE Access*, vol. 9, pp. 80535–80545, 2021, doi: 10.1109/ACCESS.2021.3084852.
- [10] Y. Chen, L. Zhang, Y. Sun, Y. He, S. W. Wong, and S. Gao, "Substrate Integrated Coaxial Line Based Continuous Transverse Stub (SICL-CTS) Array Antenna for 5G Base Station Applications," *2019 Comput. Commun. IoT Appl. ComComAp 2019*, pp. 216–219, 2019, doi: 10.1109/ComComAp46287.2019.9018777.
- [11] Y. El Hasnaoui and T. Mazri, "Study, Design and Simulation of an Array Antenna for Base Station 5G," *2020 Int. Conf. Intell. Syst. Comput. Vision, ISCV 2020*, pp. 5–9, 2020, doi: 10.1109/ISCV49265.2020.9204261.
- [12] Y. Yamada, K. Quzwain, F. Ansarudin, K. Kamardin, and N. H. Abd Rahman,

- “Aperture Antennas for 5G Mobile Base Stations,” *APACE 2019 - 2019 IEEE Asia-Pacific Conf. Appl. Electromagn. Proc.*, vol. 2, no. November, pp. 1–4, 2019, doi: 10.1109/APACE47377.2019.9021017.
- [13] P. Fernandez-Martinez, S. Martin-Anton, and D. Segovia-Vargas, “Design of a wideband vivaldi antenna for 5G base stations,” *2019 IEEE Int. Symp. Antennas Propag. Usn. Radio Sci. Meet. APSURSI 2019 - Proc.*, pp. 149–150, 2019, doi: 10.1109/APUSNCURSINRSM.2019.8888989.
- [14] Z. Dai, Y. Zhou, and J. Wang, “Design of a Broadband Base Station Antenna Based on Tightly Coupled Structure,” *2019 IEEE Int. Conf. Comput. Electromagn. ICCEM 2019 - Proc.*, pp. 1–3, 2019, doi: 10.1109/COMPEN.2019.8778852.
- [15] A. El-Bacha and R. Sarkis, “Design of tilted taper slot antenna for 5G base station antenna circular array,” *2016 IEEE Middle East Conf. Antennas Propagation, MECAP 2016*, pp. 5–8, 2016, doi: 10.1109/MECAP.2016.7790104.
- [16] J. Molins-Benlliure, A. Llanga-Vargas, D. K. Park, M. Ferrando-Bataller, and M. Cabedo-Fabres, “MIMO antenna for indoor low-band 5G base stations,” *2019 IEEE Int. Symp. Antennas Propag. Usn. Radio Sci. Meet. APSURSI 2019 - Proc.*, vol. 1, pp. 151–152, 2019, doi: 10.1109/APUSNCURSINRSM.2019.8889058.
- [17] Y. Zhao, C. Rakluea, T. Hongnara, and S. Chaimool, “A Compact Dual-Broadband Multiple-Input Multiple-Output (MIMO) Indoor Base Station Antenna for 2G/3G/LTE Systems,” *IEEE Access*, vol. 7, pp. 82238–82245, 2019, doi: 10.1109/ACCESS.2019.2924022.
- [18] J. X. Yun and R. G. Vaughan, “Multiple Element Antenna Efficiency and its Impact on Diversity and Capacity,” *IEEE Trans. Antennas Propag.*, vol. 60, no. 2, pp. 529–539, Feb. 2012, doi: 10.1109/TAP.2011.2173444.